JOURNAL OF MATERIALS SCIENCE **34** (1999) 4623–4628

X-ray diffraction and X-ray photoelectron spectra of Fe-Cr-N films deposited by DC reactive sputtering

D. L. PENG, K. SUMIYAMA, M. OKU, T. J. KONNO, K. WAGATSUMA, K. SUZUKI
Institute for Materials Research, Tohoku University, Sendai 980-8577, Japan
E-mail: peng@snap8.imr.tohoku.ac.jp

The effects of nitrogen flow ratio, target area ratio of Cr, and substrate temperature on the structure of DC reactive sputtered Fe-Cr-N ternary films have been studied. X-ray diffraction measurements show that Fe-Cr-N films consist of α-Fe(Cr) and γ'-$(Fe,Cr)_4N_x$ ($x < 1$) phases. The crystal grain of the α-Fe(Cr) phase becomes finer and a (200) texture of the γ'-$(Fe,Cr)_4N_x$ phase becomes more marked with increasing the nitrogen flow ratio. X-ray photoelectron spectra of the films show that oxidation resistance of Fe-Cr-N films is superior to that of Fe-N films, and oxides are formed only in the film surface due to contacting with the ambient atmosphere and oxygen contamination is very small in the inner parts of these films.

1. Introduction

To obtain ultra fine grains of α-Fe sputtered films, the ternary Fe-X-N ($X =$ Zr, Hf, Nb, Ta) systems in which each element X had strong affinity for nitrogen and ability of amorphous formation were investigated extensively [1–6]. Good soft magnetic properties and high saturation flux density were obtained in each system. On the other hand, the addition of the third X elements has succeeded in solving high magnetostriction and poor thermal stability of binary Fe-N film. For each ternary system, as-prepared films consisted of an amorphous-like phase and annealed films were a homogeneous mixture of fine-grained α-Fe and X (Zr, Hf, Nb, Ta) nitrides. In our previous studies on the structure, magnetic properties and thermal stability of the ternary Fe-Ti-N films deposited by DC magnetron facing target sputtering, Ti_2N phase was formed in as-prepared and annealed films [7, 8].

Recently, we reported a new ternary Fe-Cr-N film with the perpendicular magnetic anisotropy deposited by DC reactive sputtering [9]. Adjusting the chemical composition and deposition parameters, saturation magnetization of 0.37–0.5 Wb/m^2 and perpendicular coercivity of 6.4×10^4–8.8×10^4 A/m are observed for the Fe-Cr-N films.

In this paper, we report the detailed analyses of X-ray diffractions and photoelectron spectra of the Fe-Cr-N ternary films prepared at various sputter-deposition conditions.

2. Experimental

Fe-Cr-N films were deposited on glass and aluminum foil substrates by a facing-target-type DC magnetron sputtering in a mixed $Ar + N_2$ plasma, using a composite target consisting of pure Fe (99.9%) and Cr (99.9%) plates. The alloy composition was adjusted by changing the surface area ratio of Cr plates, A_{Cr}, defined as $A_{Cr} =$ (an area of Cr)/(a total area of Fe and Cr). In order to obtain Fe-Cr-N films with various nitrogen contents, a N_2 flow ratio, $R(N_2) = (N_2\text{-flow rate})/(\text{Ar-flow rate} + N_2\text{-flow rate})$, was changed by fine control of mass flow controllers. The substrate temperature, T_S, during the sputter-deposition was kept at about 50 °C by water-cooling and at 150, 250 and 350 °C by indirect resistive heating, respectively. The sputtering conditions were described elsewhere [9]. The chemical composition of deposited films was determined by inductively coupled plasma (ICP) optical emission spectrometry and helium carrier fusion-thermal conductivity methods.

X-ray diffraction (XRD) analysis of the films was performed on a conventional diffractometer with CuK_α radiation using a graphite monochromator and a film X-ray diffractometer designed according to the Seemann-Bohlin focusing principle for small incident angles. X-ray photoelectron spectra (XPS) were measured by Surface Science Laboratories model SSX-100 spectrometer with a monochromatic AlK_α source having a 300×450 μm spot size. The base pressure in the spectrometer was 1.3×10^{-7} Pa or better. Magnetic properties of the films were measured by a vibrating sample magnetometer (VSM) in a magnetic field up to 16 kOe applied parallel and perpendicular to the film plane.

3. Results

3.1. X-ray diffraction analyses

The perpendicular magnetic anisotropy of Fe-Cr-N films depends on sputter-deposition parameters [9],

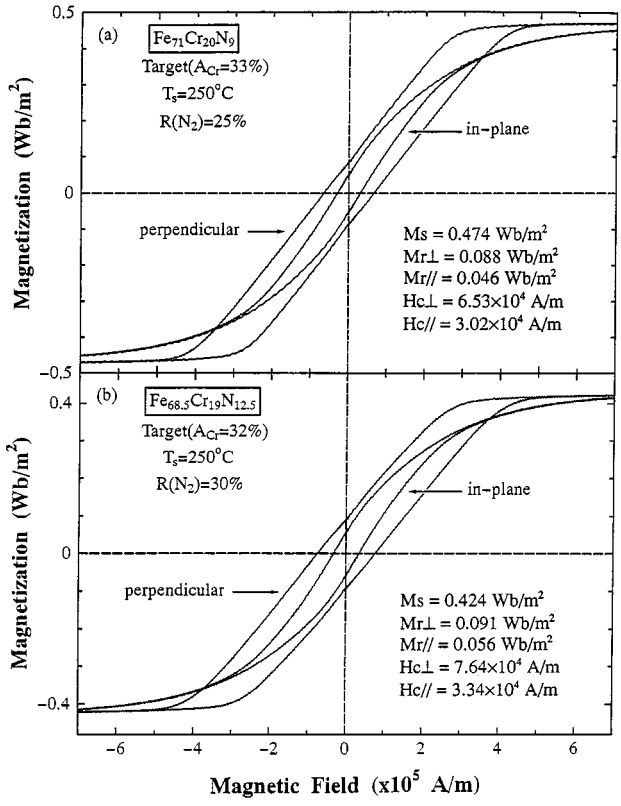

Figure 1 Magnetization curves at room temperature in magnetic fields parallel and perpendicular to the $Fe_{71}Cr_{20}N_9$ (a) and $Fe_{68.5}Cr_{19}N_{12.5}$ (b) film planes.

in particular, on $R(N_2)$, A_{Cr} and T_S. Fig. 1 shows the magnetization curves of (a) $Fe_{71}Cr_{20}N_9$ and (b) $Fe_{68.5}Cr_{19}N_{12.5}$ films of about 7 μm thickness. $H_c\perp$ is more than twice of $H_c//$, displaying large perpendicular anisotropy.

Fig. 2 shows the evolution of X-ray diffraction patterns of the films deposited at (a) $A_{Cr} = 33\%$ and (b) 35% as a function of $R(N_2)$. The X-ray diffraction patterns show similar $R(N_2)$ dependences for both films. The films consist of α-Fe(Cr) and γ'-$(Fe,Cr)_4N_x$ ($x < 1$) phases. For the α-Fe(Cr) phase, the (110) peaks broaden and their intensities become smaller as $R(N_2)$ increases. This shows a tendency of refinement of the crystal grain and piling of strain as $R(N_2)$ increases. For the γ'-$(Fe,Cr)_4N_x$ phase, the intensity of (200) peak becomes larger as $R(N_2)$ increases and the (200) texture growth becomes more remarkable. Moreover, the (200) peak of the γ'-$(Fe,Cr)_4N_x$ phase shifts to a lower 2θ side as $R(N_2)$ increases. Fig. 3a and b show the lattice constants, a, calculated from the interplanar distance, d_{200}, of the γ'-$(Fe,Cr)_4N_x$(200) peak and the nitrogen content, C_N, as a function of $R(N_2)$. C_N increases as $R(N_2)$ increases and is 18 at % at $R(N_2) = 40\%$ for $A_{Cr} = 33\%$, being smaller than the nitrogen content (20 at %) of pure γ'-Fe_4N. The a values of these films are always larger than that of pure fcc Fe, smaller than that of γ'-Fe_4N and increase with increasing $R(N_2)$. Namely, the a values are close to that of fcc Fe ($a = 3.60$ Å) for lower $R(N_2)$ and that of γ'-Fe_4N (fcc, $a =$ 3.795 Å) for higher $R(N_2)$, respectively. Therefore, the peak near $2\theta = 50^\circ$ of the X-ray diffraction pattern in Fig. 1 is allotted to γ'-$(Fe,Cr)_4N_x$(200) (with $x < 1$). On

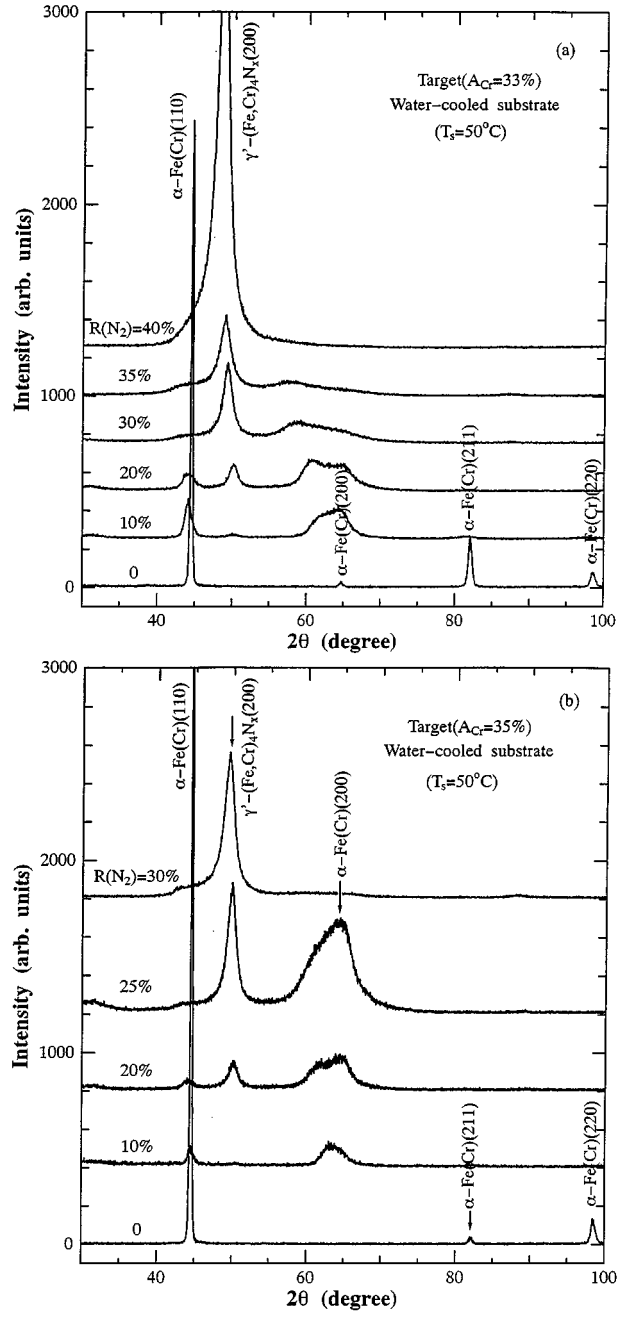

Figure 2 X-ray diffraction patterns of the Fe-Cr-N films deposited on water cooled substrates under several N_2 flow ratio ($R(N_2)$) from a composite target with area ratio: (a) $A_{Cr} = 33\%$ and (b) 35%.

the other hand, as can been seen from Fig. 2, the full width of the half maximum of the γ'-$(Fe,Cr)_4N_x$(200) peak is much wider than that of α-Fe(Cr)(110) in Fe-Cr films, being about 1.25° for $R(N_2) = 40\%$ although the intensity of the γ'-$(Fe,Cr)_4N_x$(200) peak is large. This indicates that large distortion exists in the nonequilibrium γ'-$(Fe,Cr)_4N_x$ phase due to insufficient nitrogen content (less than 20 at %). In addition, the larger A_{Cr} of the Fe-Cr composite target is, the smaller the lattice constant at the same $R(N_2)$ values. This also suggests that there is tendence of formation of the fcc-type Fe(Cr) phase with the increase of Cr content.

Fig. 4 shows the XRD patterns of the films deposited at different T_S at $R(N_2) = 30$ and 35%, respectively. The patterns of the films deposited at both $R(N_2)$ indicate the same T_S dependences. The crystal structure

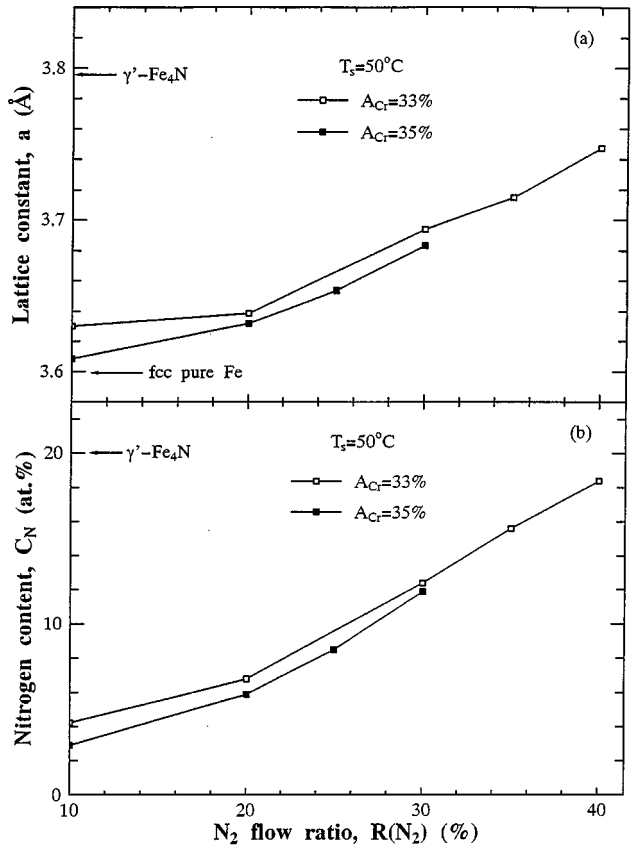

Figure 3 $R(N_2)$ dependence of lattice constant of the γ'-$(Fe,Cr)_4N_x$ phase and nitrogen content (C_N) in the Fe-Cr-N films deposited at $A_{Cr} = 33$ and 35% on water cooled substrates.

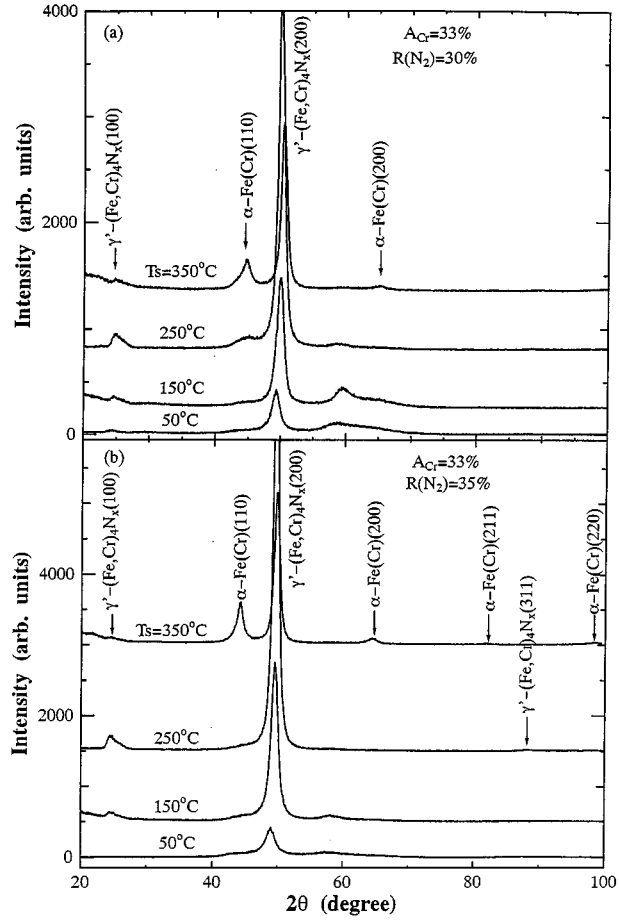

Figure 4 X-ray diffraction patterns of the Fe-Cr-N films deposited at $A_{Cr} = 33\%$ at (a) $R(N_2) = 30\%$ and (b) 35% at different substrate temperature, T_S.

change of these films is not obvious with increasing T_S up to 250 °C; the films consist of a fine-grain α-Fe(Cr) phase and a γ'-$(Fe,Cr)_4N_x$ phase with a strong (200) texture. At $T_S = 350$ °C, the (110) peak of the α-Fe(Cr) phase becomes higher and sharper and the (200) peak of the γ'-$(Fe,Cr)_4N_x$ phase lower. This indicates that the amount and grain size of the α-Fe(Cr) phase increases, comparing with those prepared at $T_S = 250$ °C. In addition, the (200) peak of the γ'-$(Fe,Cr)_4N_x$ phase shifts to the larger 2θ side as T_S increases. The lattice constants, a, are plotted versus T_S in Fig. 5. They decrease gradually with increasing T_S and are close to that of pure fcc Fe at $T_S = 350$ °C. Moreover, the a values of the films deposited at $R(N_2) = 35\%$ are always larger than those of the films at $R(N_2) = 30\%$ for the same T_S, being in agreement with $R(N_2)$ dependence at $T_S = 50$ °C (Fig. 3).

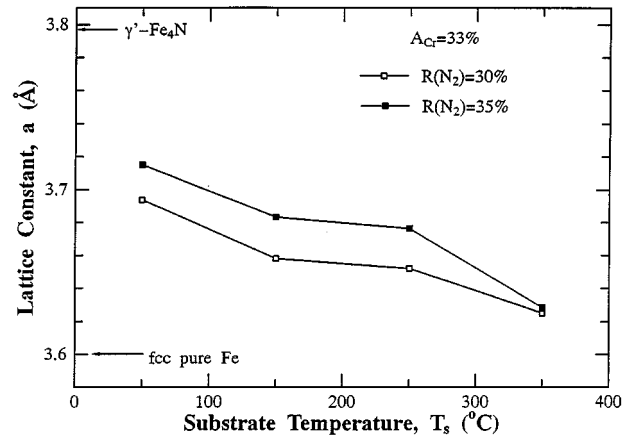

Figure 5 Substrate temperature dependence of lattice constant a of the γ'-$(Fe,Cr)_4N_x$ phase in the Fe-Cr-N films deposited at $A_{Cr} = 33\%$ and $R(N_2) = 30$ and 35%.

3.2. X-ray photoelectron spectra

Fig. 6 shows $Fe_{2p3/2}$ and $Fe_{2p1/2}$ XPS spectra of $Fe_{64}Cr_{18}N_{18}$, $Fe_{87}N_{13}$ and $Fe_{74}Cr_{26}$ films. The samples are deposited on water-cooled substrates and then exposed to air. The sample surfaces were not cleaned by Ar^+ sputtering before the XPS measurements. As can be seen, $Fe_{2p3/2}$ and $Fe_{2p1/2}$ peaks of the iron oxides are detected for all of these films. However, $Fe_{2p3/2}$ and $Fe_{2p1/2}$ peaks of metallic iron are clearly observed in Fe-Cr and Fe-Cr-N films, while they are slightly observed in Fe-N films. This indicates that oxidation resistance of Fe-Cr-N and Fe-Cr films are superior to that of Fe-N films.

Fig. 7 shows Fe_{2p} XPS spectra of the $Fe_{64}Cr_{18}N_{18}$ film as a function of Ar^+ sputter-etching time at 1 kV and 1 mA. Large amount of iron oxides are observed in the film surface of the as-deposited film, while the Fe_{2p} XPS peak of iron oxides disappear almost completely in the film sputter-etched with Ar^+ for 5 min. This indicates that the oxides are formed only in the film surface due to contacting with the ambient atmosphere

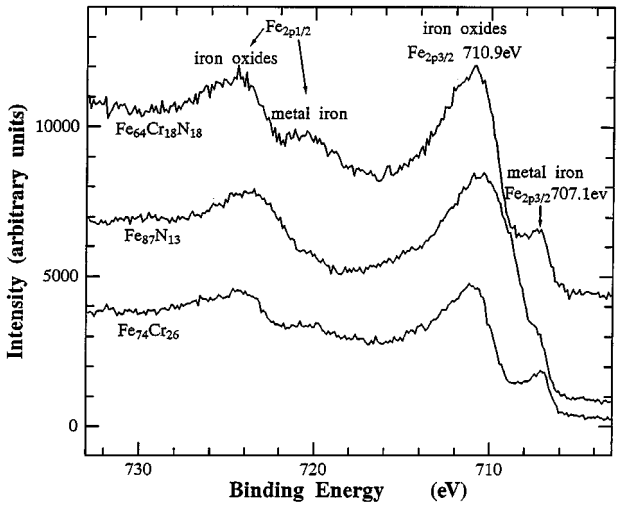

Figure 6 $Fe_{2p3/2}$ and $Fe_{2p1/2}$ XPS spectra of the $Fe_{74}Cr_{26}$, $Fe_{87}N_{13}$ and $Fe_{64}Cr_{18}N_{18}$ films whose surface were not cleaned by Ar^+ sputter-etching.

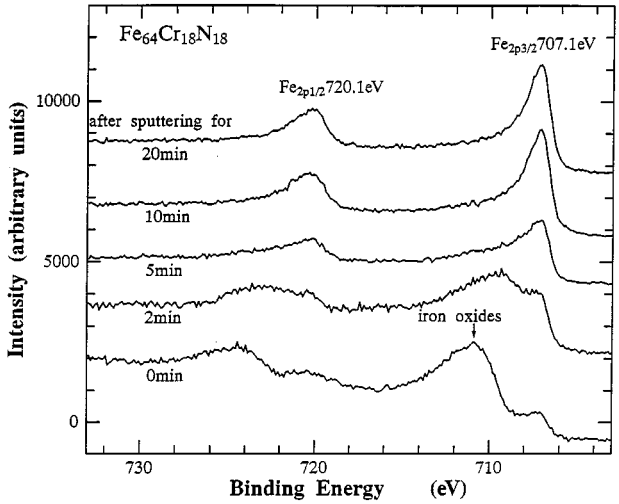

Figure 7 Time dependence of Fe_{2p} XPS spectra of $Fe_{64}Cr_{18}N_{18}$ film with Ar^+ sputter-etching at 1 kV and 1 mA.

and oxygen contamination is very small in the inner parts of these nitride films.

4. Discussion

Fig. 8 shows (a) a rocking curve of the γ'-$(Fe,Cr)_4N_x(200)$ peak for Fe-Cr-N film deposited at $R(N_2) = 40\%$ on a water-cooled substrate; (b) an XRD pattern of the crushed powder made from the sputter-deposited film; (c) an XRD pattern measured by the film X-ray diffractometer. In Fig. 8a, the full width of the half maximum is about 10°. Therefore, the (200) peak is hardly observed, when the incident angle is fixed at 2° (Fig. 8c). Because few peaks appear in X-ray diffraction patterns in Fig. 2 and the estimated lattice constant is different from those of pure fcc Fe and Fe_4N, it is very difficult to determine the structure of Fe-Cr-N films. However, this problem is solved by the measurements of X-ray diffraction shown in Fig. 8b and c, displaying several peaks of the γ'-$(Fe,Cr)_4N_x$ phase.

Moreover, the film surfaces were cleaned by Ar^+ sputtering for 10 min and the XPS measurements were

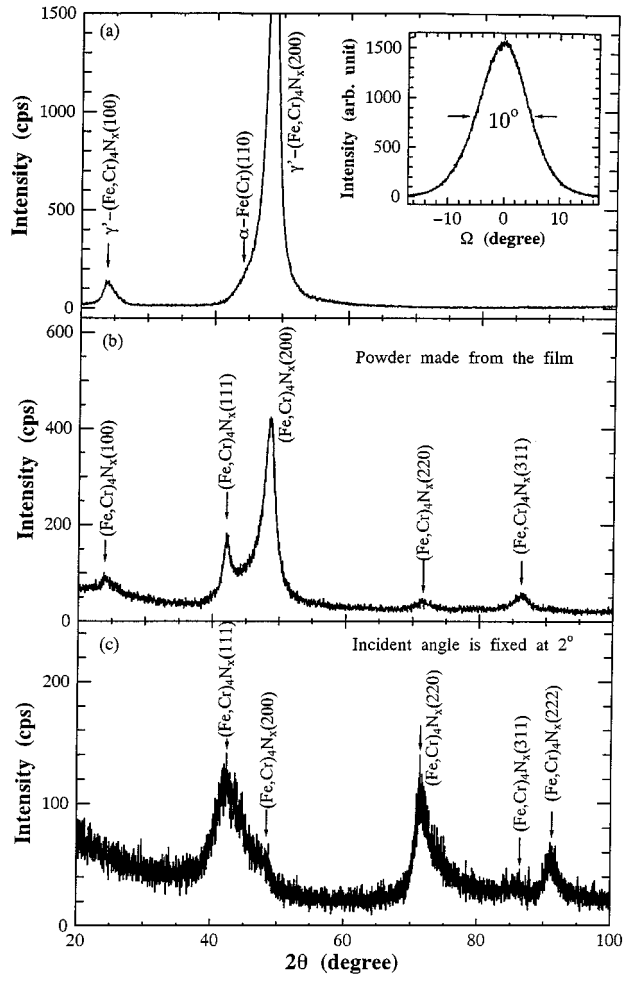

Figure 8 X-ray diffraction patterns of the Fe-Cr-N film deposited at $R(N_2) = 40\%$ on water-cooled substrate: (a) the rocking curve of the γ'-$(Fe,Cr)_4N_x(200)$ peak; (b) the result for powder made from the film; (c) the result observed by a film X-ray diffractometer.

carried out. Fig. 9 shows Fe_{2p}, Cr_{2p} and N_{1s} XPS peaks of the $Fe_{74}Cr_{26}$, $Fe_{87}N_{13}$ and $Fe_{64}Cr_{18}N_{18}$ films, whose XRD patterns are indicated in Fig. 10. The sputter-deposited $Fe_{74}Cr_{26}$ film is composed of a single α-Fe(Cr) phase, while the $Fe_{87}N_{13}$ film consists of α-Fe and γ'-Fe_4N phases, and the $Fe_{64}Cr_{18}N_{18}$ film consists of α-Fe(Cr) and γ'-$(Fe,Cr)_4N_x$ phases, respectively. As can be seen from Fig. 9a, the binding energies of $Fe_{2p3/2}$ and $Fe_{2p1/2}$ are 707.1 and 720.1 eV for these three films, being in agreement with those of metallic iron [10]. The binding energies of $Cr_{2p3/2}$ and $Cr_{2p1/2}$ (574.5 and 583.8 eV) in the Fe-Cr and Fe-Cr-N films are also the same to those of pure metallic chromium, being different from that of $Cr_{2p3/2}$ and $Cr_{2p1/2}$ (576.1 and 585.4 eV) in chromium nitrides [10]. The binding energy of N_{1s} (397.6 eV) in the Fe-Cr-N film is also in agreement with that of the Fe-N film (Fig. 8c), lower than that of the free nitrogen atoms (398.5 eV). From these results, we can propose the following two explanations. The first one is that the electronic states of Fe atoms in the iron nitride (γ'-Fe_4N) and iron-chromium nitride (γ'-$(Fe,Cr)_4N_x$) and the electron state of Cr atoms in the γ'-$(Fe,Cr)_4N_x$ are similar to those of pure metallic iron and chromium, respectively. The other is that as the film surface is sputter-etched by Ar^+ during XPS measurement, the γ'-Fe_4N and γ'-$(Fe,Cr)_4N_x$

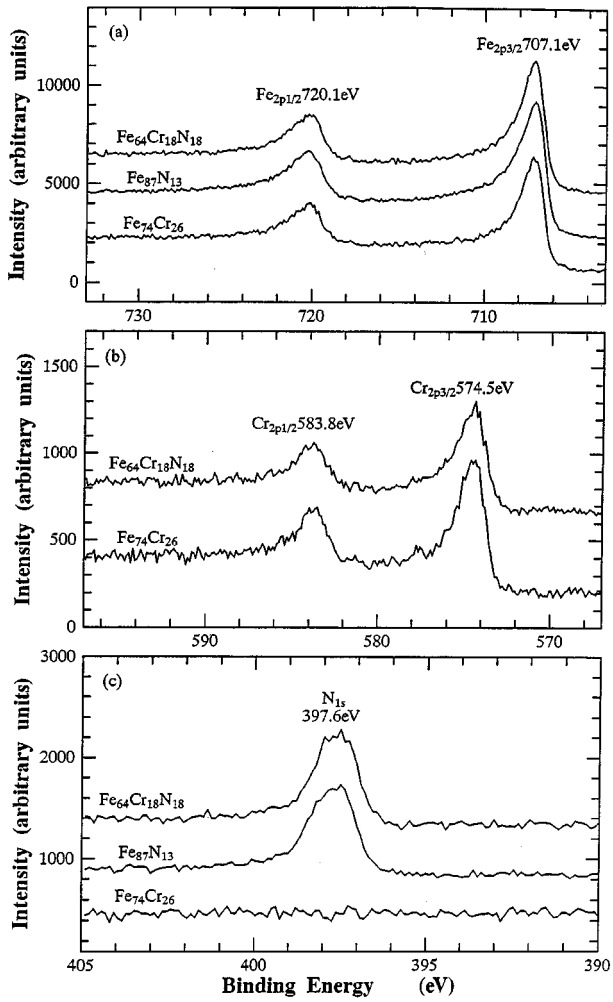

Figure 9 Fe_{2p}, Cr_{2p} and N_{1s} XPS peaks of the $Fe_{74}Cr_{26}$, $Fe_{87}N_{13}$ and $Fe_{64}Cr_{18}N_{18}$ films whose surface were cleaned by Ar^+ sputter-etching for 10 min before the XPS measurements.

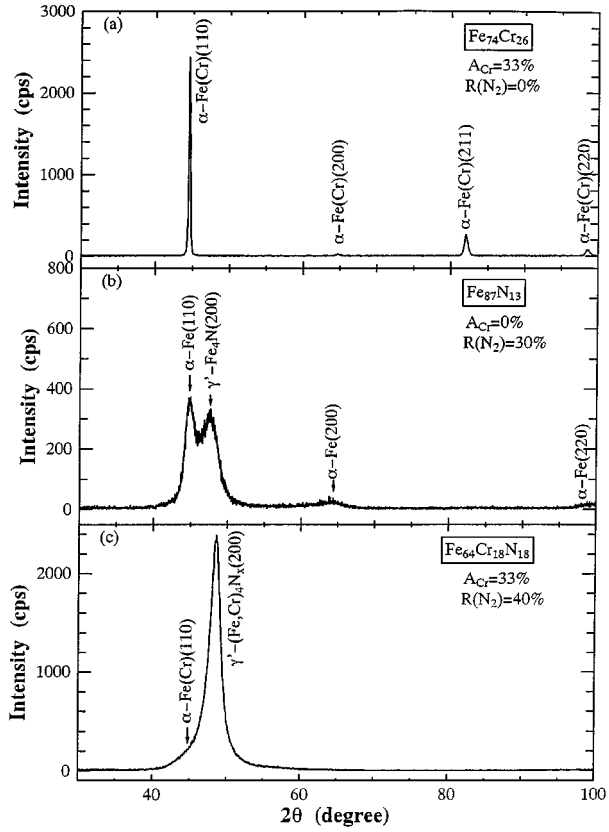

Figure 10 Comparison of X-ray diffraction patterns of the $Fe_{74}Cr_{26}$, $Fe_{87}N_{13}$ and $Fe_{64}Cr_{18}N_{18}$ films.

phases are destroyed to become metallic Fe and Cr states in which nitrogen atoms dissolve interstitiallly.

It is worth noting that though Cr content is large (about 20 at%) and the maximum nitrogen content is about 18 at% (from Fig. 3b), a chromium nitride is not formed in the sputtered Fe-Cr-N films, as can be seen from the X-ray diffraction and XPS results. This is a marked contrast to the Fe-Ti-N films deposited under same deposition conditions in which the titanium nitride, Ti_2N, is formed [7, 8]. This also suggests that Ti atoms react more preferentially with N in comparison to Cr atoms.

5. Conclusions

Fe-Cr-N ternary films with large perpendicular magnetic anisotropy have been obtained using a facing target sputtering system with the reactive atmosphere ($Ar + N_2$ mixture). From our X-ray diffraction and XPS measurements of the Fe-Cr-N, Fe-Cr and Fe-N films, We can conclude:

(1) Fe-Cr-N films consist of a mixture of the α-Fe(Cr) and γ'-$(Fe,Cr)_4N_x$ ($x < 1$) phases, whose volume fraction depends on the deposition parameters $R(N_2)$, A_{Cr} and T_S. The incorporation of N into Fe-Cr films causes the refinement of crystal grain of the α-Fe(Cr) phase and the growth of the γ'-$(Fe,Cr)_4N_x$(200) texture.

(2) The lattice constants of the γ'-$(Fe,Cr)_4N_x$ phase in the Fe-Cr-N films are always smaller than that of pure γ'-Fe_4N, and increase with increasing $R(N_2)$ and decreasing A_{Cr}, and decrease with increasing T_S.

(3) The oxidation resistance of Fe-Cr-N films are superior to that of Fe-N films, and no obvious difference in the binding energies of Fe, Cr and N is detected in the XPS spectra of the Fe-Cr-N, Fe-Cr and Fe-N films.

Acknowledgements

The authors express their appreciation to Dr. T. Takada and Mr. Y Murakami for their support of the chemical analysis. One of the author (D. L. Peng) appreciates the financial support from the Ministry of Education, Science, Culture and Sport, Japan. This work was also partially supported by Grant-in-Aid for General Scientific Research (No. 08405043) given by the Ministry of Education, Science, Culture and Sport, Japan.

References

1. Y. IITAKE and Y. SHIMADA, *J. Mag. Soc. Jpn.* **15** (1991) 361.
2. K. NAKANISHI, O. SHIMIZI and S. YOSHIDA, *ibid.* **15** (1991) 371.
3. K. NAGO, H. SAKAKIMA and K. IHARA, *ibid.* **15** (1991) 365.
4. J. C. LIN, L. J. CHEN and C. J. CHEN, *IEEE Trans. Magn.* **30** (1994) 3912.

5. G. QIU, E. HAFTEK and J. A. BARNARD, *J. Appl. Phys.* **73** (1993) 6573.
6. T. SHIMATSU, H. UWAZUMI, M. TAKAHASHI and T. WAKIYAMA, *J. Magn. Soc. Jpn.* **15** (1991) 375.
7. D. L. PENG, K. SUMIYAMA, M. OKU, D. X. LI and K. SUZUKI, *Phys. Stat. Sol. (a)* **157** (1996) 139.
8. D. L. PENG, K. SUMIYAMA and K. SUZUKI, *J. Alloys Compd.* **255** (1996) 50.
9. D. L. PENG, K. SUMIYAMA, T. J. KONNO and K. SUZIKI, *Jpn. J. Appl. Phys.* **36** (1997) L479.
10. J. F. MOULDER, W. F. STICKLE, P. E. SOBOL and K. D. BOMBEN, in "Handbook of X-ray Photoelectron Spectroscopy," edited by J. Chastain (Perkin-Elmer Corp., Physical Electronics Division, Minnesota, 1992).

Received 27 January 1997
and accepted 9 March 1999